A battery model that fully couples mechanics and electrochemistry at both particle and electrode levels by incorporation of particle interaction

Bin Wu, Wei Lu[*]

Department of Mechanical Engineering, University of Michigan, Ann Arbor, MI 48109, USA

HIGHLIGHTS

- Fully coupled mechanics and electrochemistry at both particle and electrode levels.
- Particle interaction stress acts as loads on the particle surface.
- Stress affects electrochemical reaction rates by a stress-dependent over-potential.
- A small electrochemically inactive region can cause large stress in its vicinity.
- A strategy to reduce degradation by improving the homogeneity of the electrode.

GRAPHICAL ABSTRACT
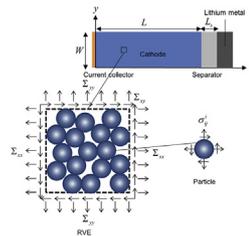
ARTICLE INFO

ABSTRACT

This paper develops a multi-scale mechanical-electrochemical model which enables fully coupled mechanics and electrochemistry at both particle and electrode levels. At the particle level, solid diffusion is modeled using a generalized chemical potential to capture the effects of mechanical stress and phase transformation. At the electrode level, the stress arising from particle interaction is incorporated in a continuum model. This particle interaction stress is in addition to the traditional concept of intercalation stress inside isolated particles. The particle and continuum electrode levels are linked by the particle interaction stress as loads on the particle surface, and by consideration of stress on the electrochemical reaction rate on the particle surface. The effect of mechanical stress on electrochemical reaction results in a stress-dependent over-potential between particle and electrolyte. Stress gradient in an electrode leads to inhomogeneous intercalation/deintercalation currents for particles depending on their interaction stress with neighbors, resulting in stress gradient induced inhomogeneous state of charge. Conversely, non-uniform intercalation/deintercalation currents in an electrode lead to stress between particles. With this model we have an important finding: an electrochemically inactive region in an electrode causes stress built-up. This model provides a powerful tool to address various problems such as fracture in-between particles.

© 2017 Elsevier B.V. All rights reserved.

1. Introduction

Mechanical degradation is one of the main causes of capacity fade in lithium-ion batteries [1]. During lithium intercalation and

* Corresponding author.
  E-mail address: weilu@umich.edu (W. Lu).

deintercalation, the active material particles of battery electrodes experience mechanical deformation, which induces stress inside particles and in-between particles. These stresses can lead to cracks and fractures of the electrode, such as cracks inside particles or in-between particles, causing isolation of active materials, disruption of the electrically conductive particle network and exposure of fresh surfaces for side reactions that result in capacity degradation [2].

Coupled electrochemical and mechanical modelling is essential to investigate stress generation and to evaluate its effect on battery performance. Prior models at the particle level mostly focused on a single, isolated particle [3—5]. Treating the intercalation-induced stress in analogy to thermal stress, a coupled electrochemical and mechanical model has been developed to study the stress and concentration field inside a particle [5]. This type of isolated particle model has been widely used and extended to address various problems [6—8], such as stress inside an agglomerate particle [9] and stress generation coupled with phase transition [10]. While these models are very useful to consider stress and fracture inside a particle, they cannot be used for problems such as fracture in-between particles since particle interaction is omitted. Mechanical stress can change the electrochemical potential of a solid and therefore (1) affects the diffusion in the solid, and (2) affects the electrochemical reaction between the solid and the electrolyte. Prior models mostly focused on stress-enhanced diffusion in a solid. For example, the developed stress gradient inside a LiMn$_2$O$_4$ particle is predicted to increase the effective solid diffusivity by up to 35% [5]. This is because both concentration gradient and stress gradient drive the diffusion flux, which is larger than the flux calculated from concentration gradient alone. Many models have followed the thermal stress analogy approach to couple the intercalation stress [8,11]. The effect of mechanical stress on the electrochemical reaction rate has not been included in most models, except in only few studies [7]. While the mechanical effect on electrochemical reaction rate may be negligible for an isolated particle, including this effect is necessary when modeling particle interaction since stress gradient in the electrode leads to spatial-dependent interaction stress between particles. It is necessary to account for different intercalation/deintercalation currents for particles under different stress states that are dependent on their interaction with neighbor particles.

In comparison to single particle level, the electrode level model coupling electrochemistry and mechanics are lacking. There have been several attempts [7,11—13] to couple the mechanical model of isolated particles [5] with the porous electrode model [14] to analyze the distribution of intercalation stresses inside different particles across the electrode. In those attempts, however, the particles are considered isolated with no interaction between them. Particle interaction can result in stress level comparable to the stress generated from the concentration gradient. In addition, the gradient from a distribution of interaction stress can lead to highly inhomogeneous interaction/deintercalation currents for particles at different locations. Several experimental works have measured the stress and strain at the electrode level and highlighted the importance of mechanical stress [15—17]. A model that is capable of capturing the stress caused by particle interaction, and fully couples electrochemistry and mechanics at both particle level and continuum electrode level, is highly demanded. In addition to more accurate prediction of battery performance, such a model is necessary to predicting inter-particle phenomena such as fracture propagation between particles.

Recently electrode microstructures constructed from focused ion beam scanning electron microscope (FIB/SEM) [18] or X-ray tomography [19] have been directly modeled using finite element methods (FEM) to investigate the microscopic electrochemical and

mechanical behaviors. Researchers have found considerable stress arising from the contact between particles [20,21], which highlights the importance to consider the interaction between particles. However, these direct numerical modeling of microstructures often incur high experimental and computational costs related to microstructure characterization and simulation. The requirement of a sufficiently large representative volume containing many microstructures to be statistically representative poses challenges on the size and the time scale of an electrode that can be practically simulated. Therefore a model that integrates electrochemistry and mechanics, and integrates the particle level and the continuum electrode level without introducing undue complexity is highly desirable to identify and interpret the mechanisms that affect battery performance, to allow for efficient parametric studies, and to guide electrode design.

The objective of this work is to develop a multi-scale and multi-physics model that integrates electrochemical and mechanical behaviors at both particle level and continuum electrode level with incorporation of particle interaction. As demonstration, we have used the model to simulate a LiMn$_2$O$_4$ half-cell, which revealed rich behaviors resulting from particle interaction and coupled electrochemistry and mechanics, and how the interaction between electrochemistry and mechanics manifests and interconnects across the two levels. We chose LiMn$_2$O$_4$ as a demonstration material system because its material parameters are available in the literature and because it exhibits phase transition during lithiation which allows us to demonstrate the capability of our model to capture the effect of phase transition. Our model is general and can be applied to various other materials, including anode materials. With this model we have found for the first time that an electrochemically inactive region in an electrode can cause significant stress built-up. The finding provides an important insight to reduce the degradation by increasing homogeneity of the electrode. This model provides a tool to study various problems related to inter-particle behaviors that cannot be addressed by the isolated particle model, such as defect growth and crack evolution in-between particles, electrode deformation and yielding, detachment of active material, or delamination of electrode from the current collector.

2. Model development

Fig. 1 illustrates the concept to model particle interaction and to link the particle level and the continuum electrode level. Each spatial point in the continuum level corresponds to a particle level representative volume element (RVE) consisting of many particles and porous volume occupied by the electrolyte. Individual particles are not visible in the continuum level. The mechanical stress in a particle comes from two sources: (1) stress induced by lithium concentration gradient inside the particle, denoted as σ_{ij}^c, and (2) stress induced by particle interaction, denoted as σ_{ij}^i. The stress σ_{ij}^c can be calculated by the lithium concentration distribution inside the particle. The expansion of a particle due to lithium intercalation is constrained by its surrounding particles. The interaction stress, σ_{ij}^i, depends on the expansion of the particle relative to that of its neighbors, as well as any macroscopic loading applied to the overall electrode. The stress in a particle is given by $\sigma_{ij}^c + \sigma_{ij}^i$. In the following sections, we first tackle diffusion in the solid and the associated σ_{ij}^c inside a particle in section 2.1. The interaction stress, σ_{ij}^i, is formulated in section 2.2.

2.1. Particle level

2.1.1. Stress

We first consider an isolated particle, where the stress arises
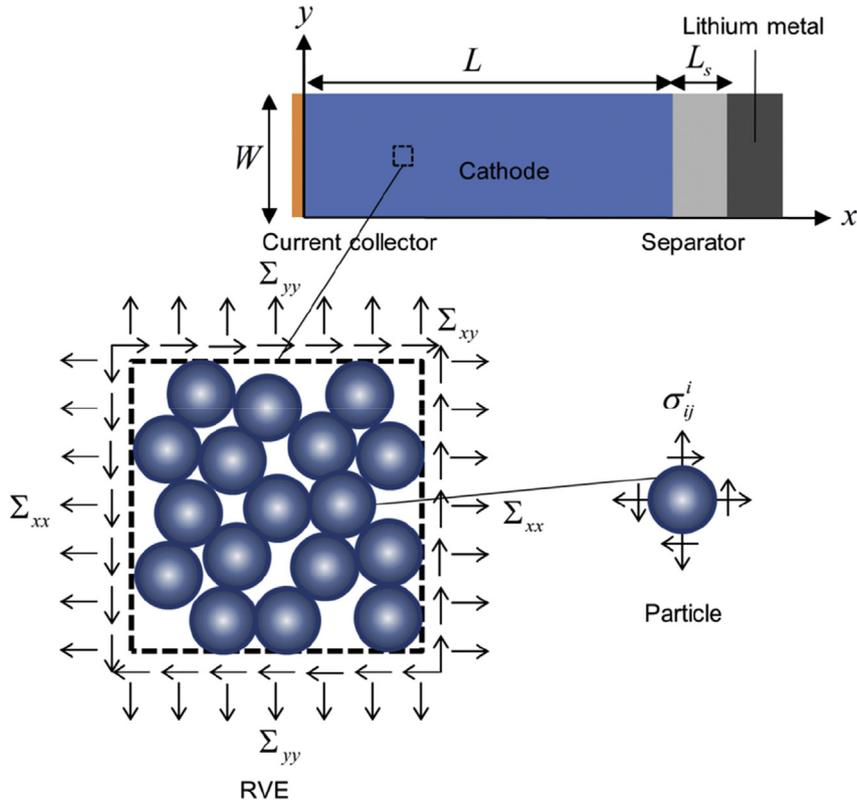
Fig. 1. Illustration of the concept to model particle interaction and to link the particle level and the continuum electrode level. Each spatial point in the electrode level corresponds to a particle level representative volume element (RVE) consisting of many particles and porous volume occupied by the electrolyte. The shade of color in the particle represents lithium concentration. The stress in a particle is the superposition of the stress due to lithium concentration gradient in the particle and the stress due to particle interaction. (For interpretation of the references to colour in this figure legend, the reader is referred to the web version of this article.)

only from the concentration gradient inside the particle. The radial and tangential strains of an isolated particle are given by Ref. [5],

$$
\varepsilon_{rr}^c = \frac{1}{E_p}\left(\sigma_{rr} - 2\nu_p\sigma_{\theta\theta}\right) + \frac{\Omega}{3}\tilde{c},
$$
$$
\varepsilon_{\theta\theta}^c = \frac{1}{E_p}\left(\sigma_{\theta\theta} - \nu_p(\sigma_{\theta\theta} + \sigma_{rr})\right) + \frac{\Omega}{3}\tilde{c},
\tag{1}
$$

where $\tilde{c} = c_s - c_{s0}$ is the difference between lithium concentration at the current state, c_s, and the initial stress-free state, c_{s0}. E_p is the Young's modulus of the active particle, σ_{rr} is the radial stress, $\sigma_{\theta\theta}$ is the tangential stress, ν_p is the Poisson's ratio of the active particle, Ω is the partial molar volume of lithium ion in the active particle.

The strains can be written as functions of the radial displacement as

$$
\varepsilon_{rr}^c = \frac{du}{dr}, \quad \varepsilon_{\theta\theta}^c = \frac{u}{r},
\tag{2}
$$

where u is the radial displacement and r is the radial coordinate.

The stress equilibrium inside the particle gives

$$
\frac{d\sigma_{rr}^c}{dr} + \frac{2}{r}\left(\sigma_{rr}^c - \sigma_{\theta\theta}^c\right) = 0.
\tag{3}
$$

The boundary conditions for an isolated active particle are given by

$$
\begin{aligned}
r = 0 &: u = 0, \\
r = r_p &: \sigma_{rr}^c = 0,
\end{aligned}
\tag{4}
$$

where r_p is the particle radius.

Combining Eqs. (1)–(4), the radial and tangential stress components are given by

$$
\sigma_{rr}^c(r) = \frac{2\Omega E_p}{3(1 - \nu_p)}\left(\frac{1}{r_p^3}\int_0^{r_p}\tilde{c}r^2 dr - \frac{1}{r^3}\int_0^r \tilde{c}r^2 dr\right),
\tag{5}
$$

$$
\sigma_{\theta\theta}^c(r) = \frac{\Omega E_p}{3(1 - \nu_p)}\left(\frac{2}{r_p^3}\int_0^{r_p}\tilde{c}r^2 dr + \frac{1}{r^3}\int_0^r \tilde{c}r^2 dr - \tilde{c}\right).
\tag{6}
$$

The hydrostatic stress resulting from lithium ion concentration is

$$
\sigma_h^c(r) = \frac{\sigma_{rr}^c + 2\sigma_{\theta\theta}^c}{3} = \frac{2\Omega E_p}{3(1 - \nu_p)}\left(\frac{1}{r_p^3}\int_0^{r_p}\tilde{c}r^2 dr - \frac{\tilde{c}}{3}\right).
\tag{7}
$$

The radial displacement at the surface of the particle is

$$
u^c(r_p) = \frac{\Omega}{r_p^2}\int_0^{r_p}\tilde{c}r^2 dr = \frac{\Omega r_p}{3}\left(c_{s,avg} - c_{s0}\right),
\tag{8}
$$

where $c_{s,avg} = (3/r_p^3)\int_0^{r_p} c_s(r)r^2 dr$ is the average lithium concentration inside the particle.

The stress components σ_{ij}^c expressed in the *xyz* coordinates are obtained by transforming the stresses in Eqs. (5) and (6) from the spherical coordinates to the *xyz* coordinates using the standard stress transformation. The hydrostatic stress, $\sigma_h^c(r)$, is invariant with coordinate transformation.

Now we consider particle interaction. Each particle can be considered to be an inclusion embedded in a matrix composed of all other particles. According the Eshelby's inclusion theory, the stress in a spherical inclusion resulting from its interaction with the matrix is uniform [22,23]. Therefore, the stress σ_{ij}^i is uniform in the particle. The interaction force on the particle surface, **t**, is given by $\mathbf{t} = \mathbf{n} \cdot \boldsymbol{\sigma}^i$, where **n** is the normal direction of the particle surface. The calculation of σ_{ij}^i will be given in section 2.2. The total stress is then given by superposition, $\sigma_{ij} = \sigma_{ij}^c + \sigma_{ij}^i$.

2.1.2. Diffusion

The lithium concentration inside the active particle is determined by

$$\frac{\partial c_s}{\partial t} + \nabla \cdot \mathbf{J} = 0. \tag{9}$$

The flux of lithium ions, **J**, is given by

$$\mathbf{J} = -Mc_s \nabla \mu, \tag{10}$$

where M is the mobility of lithium ion in the solid, and μ is the chemical potential of lithium ion in the active particle.

Taking into account the effect of mechanical stress, the chemical potential of lithium ion in the active particle is given by

$$\mu = \mu_c(c_s) - \Omega \sigma_h, \tag{11}$$

where $\mu_c(c_s)$ denotes the chemical potential at the stress-free state, and $\sigma_h = \sigma_h^c + \sigma_h^i$ is the hydrostatic stress in the particle which includes the hydrostatic stress from lithium ion concentration, σ_h^c, and the hydrostatic stress from particle interaction, $\sigma_h^i = (\sigma_{xx}^i + \sigma_{yy}^i + \sigma_{zz}^i)/3$. Equation (11) suggests that a tensile hydrostatic stress reduces the chemical potential. This is because a tensile hydrostatic stress makes it easier to accommodate the volume of lithium ions. We will show that with Eq. (11) mechanical stress brings two effects: it affects diffusion in the solid particle, and the electrochemical reaction rate between the solid and the electrolyte.

Several expressions of $\mu_c(c_s)$ have been proposed in the literature [5,24]. As the gradient of the chemical potential, rather than the chemical potential itself, drives the diffusion of lithium ion inside the solid, the explicit expression of the chemical potential is not crucial for the diffusion equation. Substituting Eq. (11) in Eq. (10), the flux of lithium ions is given by

$$\mathbf{J} = -Mc_s \left(\frac{\partial \mu_c}{\partial c_s} \nabla c_s - \Omega \nabla \sigma_h \right). \tag{12}$$

Since σ_{ij}^i is uniform inside the particle, the term $\nabla \sigma_h$ is equal to $\nabla \sigma_h^c$, which can be determined using Eq. (7).

The open circuit potential (with respect to lithium metal) of the active particle, E_{ref}, depends on the difference in chemical potential between a lithium metal (μ^θ) and the active particle (μ),

$$E_{ref} = \frac{\mu^\theta - \mu}{F}, \tag{13}$$

where F is Faraday constant. Then the term $\partial \mu_c / \partial c_s$ can be determined through the profile of the open circuit potential as

$$\frac{\partial \mu_c}{\partial c_s} = -F \frac{\partial E_{ref}}{\partial c_s} = -\frac{F}{c_{s,\max}} \frac{\partial E_{ref}}{\partial x_{Li}} = -\frac{FK}{c_{s,\max}}, \tag{14}$$

where $c_{s,\max}$ is the maximum lithium concentration in the solid, x_{Li} is the lithium fraction inside the active material, and $K = \partial E_{ref} / \partial x_{Li}$ is called thermodynamic factor. The open circuit potential and the thermodynamic factor of $Li_xMn_2O_4$ are given in Fig. 2. Note that the measurement of open circuit potential is conducted under the equilibrium state, where the lithium concentration inside the particle is uniform and the electrode is free from mechanical constraint. Thus, the open circuit potential and the thermodynamic factor shown in Fig. 2 are the values corresponding to the stress-free state.

Given that the lithium ion diffusion in the active material occurs by a vacancy mechanism, the mobility decreases with the increase of lithium concentration. With this consideration, the mobility can be expressed by Ref. [24],

$$M = M_0 \left(1 - \frac{c_s}{c_{s,\max}} \right), \tag{15}$$

where M_0 is the lithium ion mobility in the solid under the condition of dilute lithium concentration. With Eq. (7), the gradient of hydrostatic stress is

$$\nabla \sigma_h = \nabla \sigma_h^c = -\frac{2\Omega E_p}{9(1 - \nu_p)} \nabla c_s. \tag{16}$$

Considering symmetry of the spherical particle, the flux of lithium ions is along the radial direction of the particle, and is given by

$$J = D_0 \left(1 - \frac{c_s}{c_{s,\max}} \right) \left(\frac{c_s}{c_{s,\max}} \right) \left(\frac{FK}{RT} - \frac{2\Omega^2 E_p c_{s,\max}}{9(1 - \nu_p)RT} \right) \frac{\partial c_s}{\partial r}, \tag{17}$$

where $D_0 = M_0 RT$ is the diffusion coefficient, R is ideal gas constant and T is temperature.

Eqs (17) and (9), which takes the form of $\partial c_s / \partial t + (1/r^2) \partial (r^2 J) / \partial r = 0$ in the spherical coordinate, give the concentration field in the particle. The boundary and initial conditions are
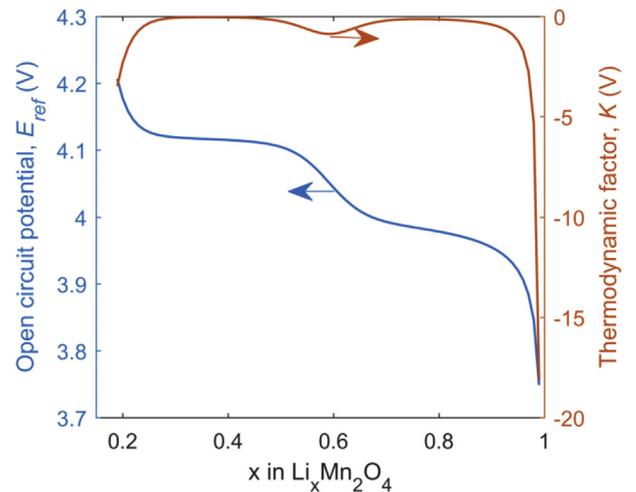
Fig. 2. Open circuit potential and thermodynamic factor profiles of LiMn₂O₄.

$$\frac{\partial c_s}{\partial r} = 0 \text{ at } r = 0,$$

$$J = \frac{i}{F} \text{ at } r = r_p, \tag{18}$$

$$c_s(r) = c_{s0} \text{ at } t = 0,$$

where i is the current density on the surface of the particle.

2.2. Electrode level

2.2.1. Electrochemistry

The classic porous electrode model assumes that the electrochemistry is homogeneous in the plane of the electrode so that an electrode can be represented by a line along the thickness direction of the electrode. This model is termed as pseudo two-dimensional (P2D) model, where one dimension is along the electrode thickness while the pseudo dimension refers to the r axis in the particle. To demonstrate the application of our model to capture defects, we will consider inhomogeneity of electrochemistry in the plane of the electrode. As shown in Fig. 1, we will consider electrochemical reaction and stress field both along the electrode thickness direction x, and the in-plane direction y. Thus the model can be called pseudo-3D. The electrode level equations are general and can be easily applied to three-dimensional electrode geometries, i.e. pseudo-4D. The two-dimensional electrode geometry in Fig. 1 enables exploration of various new problems such as the effect of defects on electrochemical reaction or fracture since these phenomena cannot be captured by one-dimensional electrode geometry.

Following the porous electrode theory, in the electrode region the potential in the solid, Φ_s, and the potential in the electrolyte, Φ_e, are governed by

$$\nabla \cdot \left(\sigma_s^{eff} \nabla \Phi_s \right) = a_s i, \tag{19}$$

$$\nabla \cdot \left\{ -\kappa_e^{eff} \left[\nabla \Phi_e - \frac{2RT}{F} \left(1 + \frac{d \ln f_{\pm}}{d \ln c_e} \right) (1 - t_+) \nabla \ln c_e \right] \right\} = a_s i, \tag{20}$$

where $\sigma_s^{eff} = \sigma_{s0} \varepsilon_s^{1.5}$ is the effective solid conductivity, σ_{s0} is the bulk solid conductivity and ε_s is the volume fraction of solid; $\kappa_e^{eff} = \kappa_{e0} \varepsilon_e^{1.5}$ is the effective electrolyte conductivity, κ_{e0} is the bulk electrolyte conductivity and ε_e is the volume fraction of electrolyte; $a_s = 3\varepsilon_s/r_p$ is the active surface area per unit electrode volume; c_e is the lithium ion concentration in the electrolyte; t_+ is the lithium ion transference number; and $f_{\pm}$ is the electrolyte activity coefficient.

Lithium ion concentration in the electrolyte is given by

$$\varepsilon_e \frac{\partial c_e}{\partial t} + \nabla \cdot \left(-D_e^{eff} \nabla c_e \right) = \frac{(1 - t_+)}{F} a_s i, \tag{21}$$

where $D_e^{eff} = D_{e0} \varepsilon_e^{1.5}$ is the effective diffusivity of the electrolyte and D_{e0} is the bulk electrolyte diffusivity.

The current density between the solid and the electrolyte is determined by the Bulter-Volmer equation,

$$i = i_0 \left(\exp\left(\frac{\alpha F \eta}{RT} \right) - \exp\left(-\frac{(1 - \alpha) F \eta}{RT} \right) \right), \tag{22}$$

where i_0 is the exchange current density, α is the anodic charge transfer coefficient and η is the over-potential.

The exchange current density is given by

$$i_0 = Fk c_{s,\text{surf}}^{1-\alpha} c_e^{\alpha} \left(c_{s,\max} - c_{s,\text{surf}} \right)^{\alpha}, \tag{23}$$

where k is the reaction rate constant and $c_{s,\text{surf}}$ is the lithium concentration at the particle surface. While rigorously speaking stress can possibly influence the exchange current density by adding to Eq. (23) a prefactor different but very close to 1, this effect is typically negligible. The effect of mechanical stress on the reaction current density between the solid and the electrolyte is reflected in the over-potential, η.

The over-potential at the particle surface is given by

$$\eta = \Phi_s - \Phi_e - E_{ref}. \tag{24}$$

With consideration of the hydrostatic stress, we have

$$E_{ref} = E_{ref}(c_s) + \frac{\Omega \sigma_h}{F}, \tag{25}$$

and

$$\eta = \Phi_s - \Phi_e - E_{ref}(c_s) - \frac{\Omega \sigma_h}{F}. \tag{26}$$

Note that the hydrostatic stress plays an important role in the over-potential. Consequently, the lithium intercalation rate at the particle surface in our model is more accurate than the prediction from a pure electrochemical model. More importantly, this stress-dependent over-potential is necessary to capture the effect of interaction stress gradient on lithium ion flux. To explain the concept, consider a flow of lithium ions toward two particles for lithium intercalation. Assume that the two particles initially have no lithium inside so that the stress comes all from particle interaction. The particle with a larger hydrostatic stress (tension is positive) exerted by its neighbors is prone to accept more lithium ions. This effect results in differential lithium flux toward the two particles. For an electrode, this effect will lead to a distribution of lithium ions in the particles affected by their interaction stress with neighbors.

The electrolyte potential and concentration in the separator region can be obtained by simply setting the right hand side of Eqs. (20) and (21) to be zero, and replacing the porosity, ε_e, by that in the separator region, $\varepsilon_{e,sep}$. The concentration, lithium ion flux, potential and current density are continuous in the electrolyte across the boundary between the electrode and the separator regions.

The boundary and initial conditions for the electrolyte concentration are

$$D_e^{eff} \frac{\partial c_e}{\partial x} = \frac{i_{app}(1 - t_+)}{F} \text{ at } x = L + L_s,$$

$$\frac{\partial c_e}{\partial x} = 0 \text{ at } x = 0,$$

$$\frac{\partial c_e}{\partial y} = 0 \text{ at } y = 0 \text{ and } y = W, \tag{27}$$

$$c_e(x, y) = c_{e0} \text{ at } t = 0,$$

where i_{app} is the applied current density with the sign defined as $i_{app} > 0$ for discharge, and c_{e0} is the initial lithium ion concentration in the electrolyte.

The boundary conditions for the solid potential are

$$\sigma_s^{eff}\frac{\partial \Phi_s}{\partial x} = i_{app} \text{ at } x = 0,$$

$$\frac{\partial \Phi_s}{\partial x} = 0 \text{ at } x = L, \qquad (28)$$

$$\frac{\partial \Phi_s}{\partial y} = 0 \text{ at } y = 0 \text{ and } y = W.$$

The boundary conditions for the electrolyte potential are

$$\frac{\partial \Phi_e}{\partial x} = 0 \text{ at } x = 0,$$

$$\frac{\partial \Phi_e}{\partial y} = 0 \text{ at } y = 0 \text{ and } y = W. \qquad (29)$$

In order to set the boundary condition at $x = L + L_s$, we first evaluate the over-potential at the surface of the lithium metal

$$\eta_{Li} = \Phi_{Li} - \Phi_e(x = L + L_s) - E_{Li}, \qquad (30)$$

where the solid potential of the lithium metal, Φ_{Li}, is set to zero. The open-circuit potential of this reaction, E_{Li}, is also zero since lithium metal is taken as the reference. The current density at the surface is

$$i_{Li} = i_{Li,0}\left(\exp\left(\frac{\alpha F \eta_{Li}}{RT}\right) - \exp\left(-\frac{(1-\alpha)F\eta_{Li}}{RT}\right)\right) \qquad (31)$$

where $i_{Li,0}$ is the exchange current density for the reaction. The conservation of charge requires that

$$i_{Li} = i_{app}. \qquad (32)$$

The electrolyte potential at $x = L + L_s$ is determined by combining Eqs. (30)–(32). It was reported that $i_{Li,0}$ is much higher than the applied current density, i_{app} [7]. Thus, a simplified approximate boundary condition is used, which is given by

$$\Phi_e = 0 \text{ at } x = L + L_s. \qquad (33)$$

2.2.2. Mechanics

Electrochemical modeling of the porous electrode, as presented in section 2.2.1, is based on the volume averaging method. This method describes the physical processes in the porous electrode through the homogenization of the solid and the electrolyte phases, thus requiring only effective properties without need to describe detailed microstructures of the electrode. The properties, such as the effective electrolyte diffusivity and conductivity, are usually determined through the Bruggeman's relation, which is primarily based on the porosity of the electrode. Compared with direct numerical simulation of microstructural details, the volume averaging method greatly reduces the computational cost and achieves satisfied accuracy. Our mechanical model will be based on the volume averaging method, which is consistent with the electrochemical model. Each spatial point in the continuum level corresponds to a particle level RVE consisting of many particles and porous volume occupied by the electrolyte.

Conceptually, the strain in a solid particle induced by lithium intercalation behaves like a thermal strain. The concentration is analogous to temperature, and the partial molar volume of lithium ion is analogous to the coefficient of thermal expansion, as can be observed in Eq. (1). Similar concept can be used to consider the eigenstrain of a RVE of the electrode, where the average lithium ion concentration in the RVE is analogous to temperature, while an "effective" partial molar volume is analogous to the coefficient of thermal expansion. A RVE may have an "effective" partial molar

volume different from that of a solid particle since the REV is porous and only the active particles in the RVE are associated with the intercalation induced strain. The relation between the partial molar volume of a RVE and a solid particle is analogously to the relation between the thermal expansion coefficient of a porous solid and a bulk solid, which has been of great interest in thermo-elasticity and poro-elasticity [25–27]. Studies have shown that the thermal expansion coefficient of a homogeneous and isotropic porous material is equal to the thermal expansion coefficient of the solid phase [26]. For heterogeneous porous materials, few experimental results show a dependence of the drained thermal expansion coefficient on porosity [26]. Theoretical derivations indicate that the drained thermal expansion coefficient is independent on the porosity if the drained compressibility is independent on temperature [25,26]. Translating these into our problem, we can consider that the "effective" partial molar volume of a RVE, Ω_e, is equal to the partial molar volume of a solid particle, i.e. $\Omega_e = \Omega$.

Thus, the eigenstrain of the RVE, $e_{ij}^0 = e^0\delta_{ij}$, can be written in terms the volumetric strain of its constituent particles. Here δ_{ij} is the Kronecker delta. According to Eq. (8), we have

$$e^0 = e_{xx}^0 = e_{yy}^0 = e_{zz}^0 = \frac{u(r_p)}{r_p} = \frac{\Omega}{3}\left(c_{s,avg} - c_{s0}\right). \qquad (34)$$

The effective Young's modulus, E, and Poisson's ratio, ν, of the composite electrode can be determined from those of solid particles using many methods, including self-consistent method [28], Mori-Tanaka method [29,30] and finite element method [31]. In this work, we use the fitted equations from finite element simulations [31],

$$E = E_p\left(1 - \frac{\varepsilon_e}{\varepsilon_0}\right)^n,$$

$$\nu = \nu_0 + \left(1 - \frac{\varepsilon_e}{\varepsilon_1}\right)^m (\nu_p - \nu_0), \qquad (35)$$

The suggested values are $\varepsilon_0 = 0.652$, $n = 2.23$, $\varepsilon_1 = 0.500$, $m = 1.22$ and $\nu_0 = 0.140$ for the porous structure consisting of connected solid spheres. The calculated elastic modulus from Eq. (35) are comparable to the results from the self-consistent method, and fall inside the Hashin and Shtrikman bounds [32].

The macroscopic stress in the electrode level, Σ_{ij}, is given by

$$\Sigma_{ij} = C_{ijkl}\left(e_{kl} - e^0\delta_{kl}\right), \qquad (36)$$

where $C_{ijkl} = \lambda\delta_{ij}\delta_{kl} + \mu(\delta_{ik}\delta_{jl} + \delta_{il}\delta_{jk})$ is the effective elastic modulus, where $\lambda = E\nu/[(1+\nu)(1-2\nu)]$ and $\mu = E/[2(1+\nu)]$ can be obtained from Eq. (35), and e_{kl} is the strain.

The equilibrium of stress gives

$$\nabla \cdot \mathbf{\Sigma} = 0 \qquad (37)$$

The boundary conditions are given by

$$u_x = u_y = 0 \text{ at } x = 0,$$
$$\Sigma_{xx} = \Sigma_{xy} = 0 \text{ at } x = L, \qquad (38)$$
$$u_y = 0 \text{ at } y = 0 \text{ and } y = W.$$

The boundary condition $\Sigma_{xx} = \Sigma_{xy} = 0$ at $x = L$ is because the separator is much more compliant than the electrode so that the electrode can deform freely toward or away from the separator.

The model described by Eqs. (34)–(38) is equivalent to a thermo-elastic problem, where the coefficient of thermal expansion is $\Omega/3$, the temperature is $c_{s,avg}$ and the initial temperature is c_{s0}. The stress field can be obtained using the finite element method. This electrode level mechanical model couples with the

electrochemical model through the average concentration.

Now we establish the relation between Σ_{ij} and the interaction stress σ_{ij}^i. Based on volume average, we have

$$\Sigma_{ij} = \varepsilon_s \left\langle \sigma_{ij}^c + \sigma_{ij}^i \right\rangle_p + \varepsilon_b \langle \sigma_{ij} \rangle_b = \varepsilon_s \sigma_{ij}^i, \tag{39}$$

where $\langle \sigma_{ij}^c + \sigma_{ij}^i \rangle_p$ is the volume average of stress over the particles, $\langle \sigma_{ij} \rangle_b$ is the volume average of stress over the binder and additives, and $\varepsilon_b = 1 - \varepsilon_s - \varepsilon_e$ is the volume fraction of the binder and additives. Note that $\langle \sigma_{ij}^c \rangle_p = 0$ since the concentration induced stress field in the particle is self-equilibrium, and $\langle \sigma_{ij}^i \rangle_p = \sigma_{ij}^i$ since σ_{ij}^i is uniform in the particle. The active particles constitute the backbone of the electrode and have much larger volume fraction and stiffness than the binder and additives, so we can neglect the $\varepsilon_b \langle \sigma_{ij} \rangle_b$ term in Eq. (39). Thus we have

$$\sigma_h^i = \frac{\Sigma_{xx} + \Sigma_{yy} + \Sigma_{zz}}{3\varepsilon_s}. \tag{40}$$

2.3. Parameters

Table 1 lists the parameters for a LiMn$_2$O$_4$ half-cell. These parameters were used in all the simulations in this paper unless specifically noted otherwise. The model was implemented using the finite element software package COMSOL Multiphysics. A simulation took 1–2 h using a regular workstation. Compared with the direct microstructural modeling which took 27 days on a cluster [33], the computational cost was much less.

3. Results

3.1. Particle level concentration and stress

Fig. 3(a) shows the radial distribution of lithium concentration

Table 1
Parameters used in the simulations.

Parameter	Symbol	Value
Electrode Level		
Cathode thickness	L	50 µm
Separator thickness	L_s	20 µm
Initial lithium ion concentration in electrolyte	c_{e0}	1000 mol m^{-3}
Cathode porosity	ε_e	0.48
Separator porosity	$\varepsilon_{e,sep}$	0.39
Volume fraction of active material	ε_s	0.42
Lithium ion transference number	t_+	0.38
Solid electronic conductivity [11]	σ_{s0}	10 S m^{-1}
Electrolyte conductivity [11]	κ_{e0}	1 S m^{-1}
Diffusivity of lithium ions in bulk electrolyte [11]	D_{e0}	3.23×10^{-10} m^2 s^{-1}
Temperature	T	298 K
Activity coefficient term	$1 + \frac{d \ln f_\pm}{d \ln c_e}$	2.83
Anodic charge transfer coefficient	α	0.5
Particle Level		
Particle radius	r_p	5 µm
Diffusivity of lithium ions in solid	D_0	1×10^{-14} m^2 s^{-1}
Reaction rate constant [11]	k	5×10^{-10} m$^{2.5}$ mol$^{-0.5}$ s^{-1}
Maximum lithium concentration in solid [11]	$c_{s,max}$	24161 mol m^{-3}
Initial lithium concentration in solid [11]	c_{s0}	0.19 $c_{s,max}$
Young's modulus of the solid particle [5]	E_p	10 GPa
Poisson's ratio of the solid particle [5]	ν_p	0.3
Lithium ion partial molar volume [5]	Ω	3.497×10^{-6} m^3 mol^{-1}

at different intercalation times in a particle close to the separator ($x = L, y = 0$ in Fig. 1). During 50–300 s, a sharp concentration jump moves from close to the surface ($r/r_p = 1$) toward the center ($r/r_p = 0$) of the particle. This jump corresponds to phase transition at the open circuit potential (OCP) plateau of 4.15 V shown in Fig. 2. After 300 s, the concentration jump associated with the OCP plateau vanishes, while a diffusional concentration gradient gradually develops until the end of discharge. The radial and tangential stresses associated with lithium concentration distribution in the particle, as indicated in Eqs. (5) and (6), are shown in Fig. 3(b) and (c). The concentration jump observed at 300 s results in large radial and tangential stresses especially at the central region of the
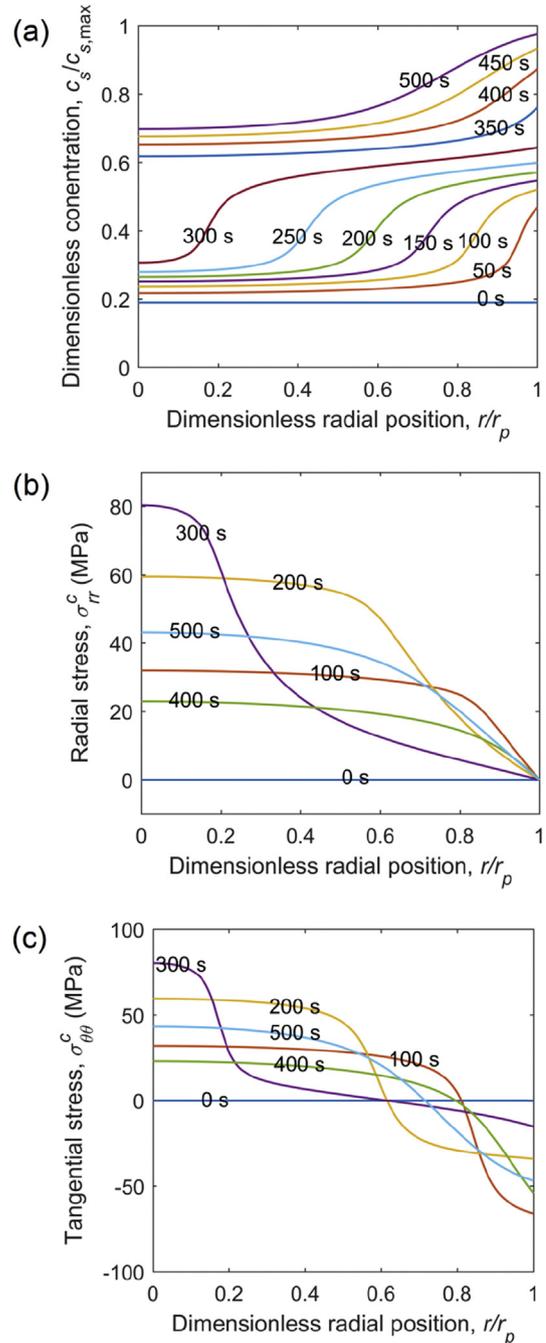
Fig. 3. Simulation results of (a) dimensionless solid concentration, (b) radial stress, (c) tangential stress inside a particle next to the separator at different intercalation (discharge) times.

particle, while vanishing of the jump reduces the stresses. The inclusion of phase transition during intercalation/deintercalation in our model by using electrochemical potential from experimental OCP and thermodynamic factor curves allows accounting for the concentration jump associated with phase transition. This approach is necessary since the concentration jump greatly increases the stresses inside a particle.

Fig. 4(a) shows the lithium concentration distribution inside all particles at time 300 s. The two horizontal axes represent the position of the particle in the electrode by the x position along the electrode thickness direction and by the y position in the plane of the electrode. The vertical axis represents a point in the particle by the radial r position. It can be observed that the concentration distribution is independent of the y axis, thus the result along $y = 0$ is plotted in Fig. 4(b)–(d). Fig. 4(b) shows that for particles along the electrode thickness similar concentration distribution, including the characteristic concentration jump, is developed. However, the jump happens closer to the center of the particle ($r/r_p = 0$) in those particles near the separator ($x/L = 1$) than those near the current collector ($x/L = 0$). This is understandable since the particles near the separator undergo lithium intercalation first when lithium ions move across the separator. Thus the concentration jump has more time to move closer to the center of the particles. Fig. 4(c) and (d) shows the distributions of radial and tangential stress at 300 s, which result from the distribution of lithium concentration.

The maximum stress is important to evaluate the mechanical integrity of the particle. The temporal profile of maximum radial and tangential stresses in particles at two representing locations, one next to the separator and the other next to the current collector, are shown in Fig. 4(e). The symbol σ_{rr}^c in Fig. 4(e) denotes the maximum tensile radial stress located at the center of a particle,

$$\sigma_{rr}^c(r = 0) = \frac{2\Omega E_p}{3(1 - \nu_p)} \left(\frac{1}{r_p^3} \int_0^{r_p} \tilde{c} r^2 dr - \frac{\tilde{c}(r = 0)}{3} \right), \tag{41}$$

while the $\sigma_{\theta\theta}^c$ in Fig. 4(e) denotes the maximum compressive tangential stress located at the surface of a particle,

$$\sigma_{\theta\theta}^c(r = r_p) = \frac{\Omega E_p}{3(1 - \nu_p)} \left(\frac{3}{r_p^3} \int_0^{r_p} \tilde{c} r^2 dr - \tilde{c}(r = r_p) \right). \tag{42}$$

The maximum radial stress peaks at the time of about 300 s for the particles next to the separator (σ_{rr}^c SP), while there is a time lag for the maximum radial stress to peak for the particle next to the current collector (σ_{rr}^c CC). This peak of stress corresponds to the concentration jump. The time lag is consistent with the difference in radial locations of the concentration jump for particles next to the separator and for particles next to the current collector, as can be observed in Fig. 4(b). The decrease of the maximum radial stress after 300 s results from the vanishing of the concentration jump.

The maximum compressive tangential stress peaks at the time of about 50 s for the particles next to separator ($\sigma_{\theta\theta}^c$ SP), which is much earlier than the peak of the maximum radial stress, σ_{rr}^c SP. This is because the maximum compressive occurs at the surface of the particle while the maximum tensile occurs at the center of the particle, and the concentration jump develops first at the surface. The lag between the peak of the $\sigma_{\theta\theta}^c$ SP curve and the peak of the σ_{rr}^c SP curve represents the time taken for the concentration jump to move from the surface to the center of the particles.

3.2. Electrode level intercalation current and stress

The intercalation current per unit volume between the solid and the electrolyte at a spatial point in the electrode is given by $a_s i$. For a given electrode a_s is a constant, therefore we focus on the current density per area at the particle surface, i. Fig. 5(a) shows the time evolution of current density at particle surfaces for those particles located next to the current collector (CC) and next to the separator (SP). The negative current means intercalation. An oscillation of the current density can be observed. The mechanism behind this oscillation can be understood below. The current density depends on the over-potential and the exchange current density, which are shown in Fig. 5(b) and (c). The oscillation pattern of the current density appears synchronized with the pattern of the over-potential, which is consistent with Eq. (22). A large magnitude of over-potential, $|\eta|$, causes a large magnitude of current density $|i|$, i.e. larger lithium intercalation rate. This leads to an increase of lithium concentration, and correspondingly a decrease of the open circuit potential E_{ref} since it depends on lithium concentration as shown in Fig. 2. According to Eq. (24), the decrease of E_{ref} results in an increase in η or a decrease in the magnitude $|\eta|$ because η is negative ($\eta < 0$ during cathode intercalation, i.e. discharge of the cell). This negative feedback mechanism causes the current density to oscillate. In this process the dependence of the open circuit potential variation on the lithium concentration variation, which is characterized by the thermodynamic factor, plays an important role. A larger magnitude of the thermodynamic factor results in a stronger negative feedback. Take the two peaks of the SP curve in Fig. 5(a) as an example. These two peaks of magnitude appear at the time of about 40 s and 350 s. According to Fig. 3(a), the dimensionless surface concentrations at these two times are roughly 0.4 and 0.75, which are consistent with where the magnitude of the thermodynamic factor in Fig. 2 minimizes.

Fig. 5(d) shows the maximum, minimum and average current density at particle surfaces by calculating the values for all particles across the electrode thickness. The maximum and minimum curves are labeled based on magnitude. An oscillation of the maximum and minimum current density can be observed, while the average current density is nearly constant due to the boundary condition of constant current discharge. Ideally, we hope that the particles across the electrode thickness intercalate at the same rate to avoid inhomogeneous degradation. However, the oscillation of current density in Fig. 5(d) shows that the real situation is different. A larger oscillation indicates more inhomogeneous intercalation current. The curves in Fig. 5(d) appear to correlate well to the curves in Fig. 5(a), suggesting that the maximum and the minimum current densities are located next to the current collector or next to the separator. Inside the electrode the current density is bounded by the maximum and minimum curves.

The distribution of electrode level stress at the end of discharge is shown in Fig. 6(a). Note that Σ_{yy} and Σ_{zz} are the same based on the boundary condition of $u_y = 0$ at $y = 0$ and $y = W$, and the plane strain calculation for the electrode. The stress Σ_{xx} is zero because of the zero force boundary condition of the electrode at the separator side. As shown in Fig. 6(b), the particles next to the separator undergo a larger compressive electrode level stress. This is a result of stronger particle interaction associated with larger volume expansion of these particles due to higher lithium concentration. While the electrode level stress appears small in comparison to the particle level stress, this electrode level stress can cause severe failure between particles by inter-particle fracture or yielding: the bonding between particles is much weaker than the cohesion of atoms inside particles, and large local stress concentration can emerge between interacting particles.

The effect of stress on over-potential can be evaluated using Eq.
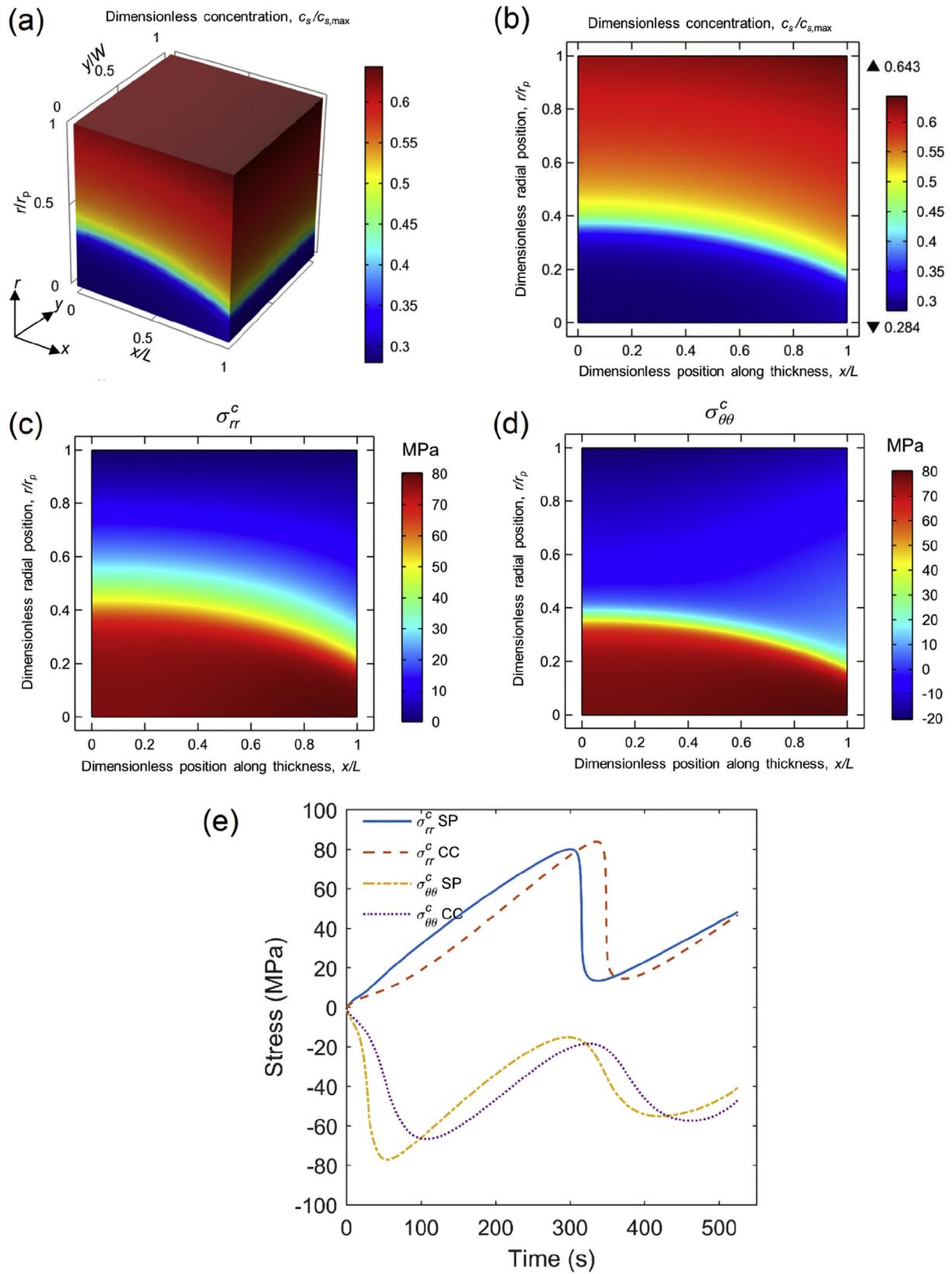
Fig. 4. (a) Distribution of lithium concentration inside all particles. Horizontal axes represent particle location in the electrode by the *x* position along the electrode thickness direction and by the *y* position in the plane of the electrode. The vertical axis represents a point in the particle by the radial *r* position; (b) Lithium concentration in particles at *y* = 0. (c) Radial stress distribution in particles (d) Tangential stress distribution in particles. Results shown are at the instant of 300 s. (e) Temporal profiles of the maximum tensile radial stress (σ_{rr}^c at particle center) and the maximum compressive tangential stress ($\sigma_{\theta\theta}^c$ at particle surface) for particles next to the separator (SP) and next to the current collector (CC).
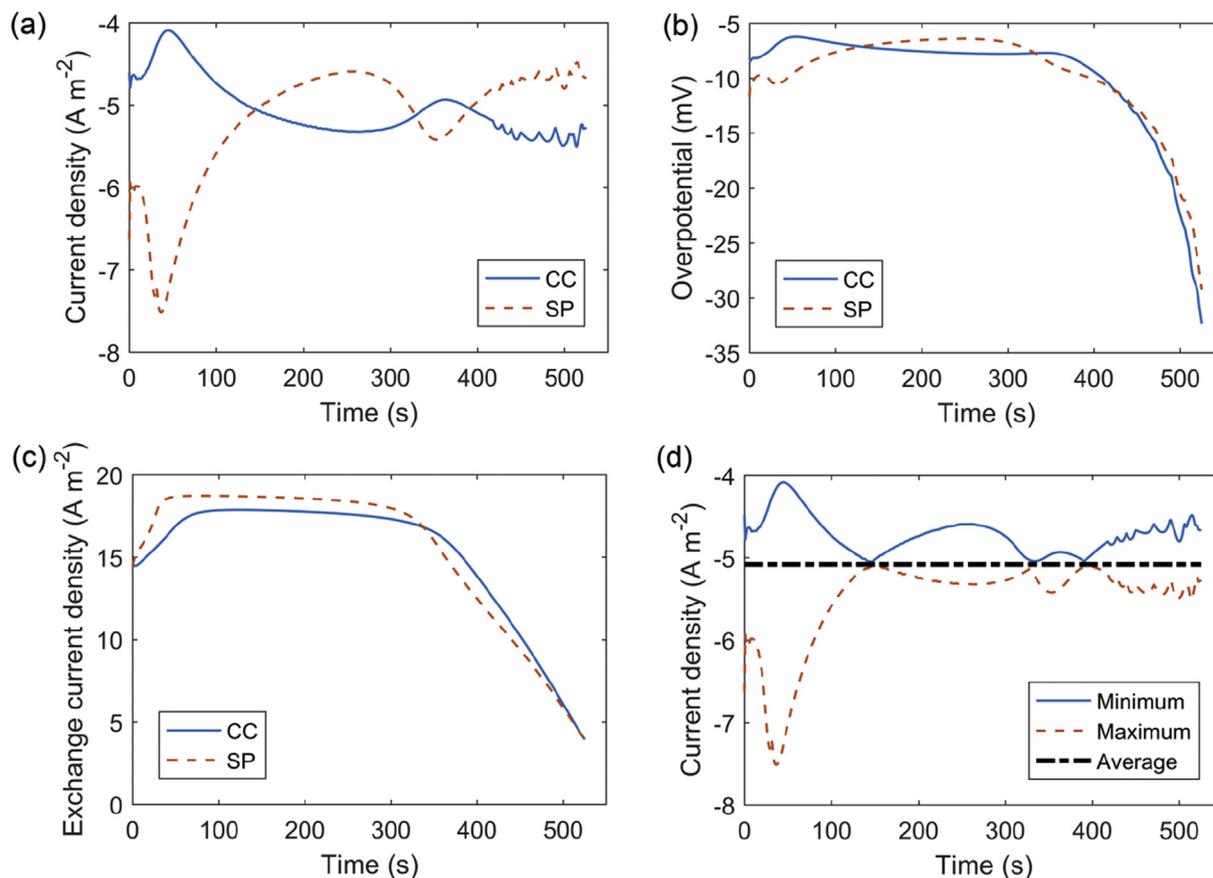
Fig. 5. Evolution of (a) current density, (b) over-potential, and (c) exchange current density at the surface of particles next to the current collector (CC) and next to the separator (SP). (d) The maximum, minimum and average current density of all particles across the electrode thickness.

(26). The largest hydrostatic stress level is about −50 MPa in the simulation, which leads to a change of 1.8 mV in the over-potential. This change accounts for 20%−30% of the maximum amplitude of over-potential before 400 s shown in Fig. 5 (b), indicating the importance to include the effect of stress on over-potential.

3.3. Effect of particle size

To investigate the effect of particle size on the electrochemical and mechanical behaviors, we simulated a case where the particle radius is 1 μm instead of 5 μm. As shown in Fig. 7(a), the lithium concentration inside each particle is fairly uniform due to the small particle radius, whereas particles along the electrode thickness show significant difference in concentration. This distribution is in sharp contrast to that in Fig. 4(a), where the particle radius is 5 μm. Consequently, the radial stress shown in Fig. 7(b) is much smaller than that in Fig. 4(c).

Smaller particle size leads to more uniform lithium distribution, thus more lithium ions intercalate into the particles at the end of discharge. Higher lithium concentration leads to larger particle expansion, thus larger electrode level stress in Fig. 7(c) as a comparison to that in Fig. 6(a).

3.4. Stress and failure induced by an electrochemically inactive region

Some small local regions in a composite electrode may lose their activity due to disruption of the electronic network, local dry up of

electrolyte, blocking of the particle surface, or other fabrication defects. These existing electrochemically inactive regions have not received any attention so far since their volume is very small. By volume of the active material, these small inactive regions have negligible impact on capacity. With the model developed in this paper, we investigated the effect of an electrochemically inactive region, and founding that it can cause large electrode level stress even though the region itself does not participate in any electrochemical reaction. This stress can further induce various electrode failures such as crack or yielding.

We put an inactive region close to the separator, as shown in Fig. 8(a). The solid particles inside the inactive region have no lithium intercalation, and thus no intercalation induced deformation. The lithium flux and current in the solid and electrolyte normal to the boundary of the inactive region are zero. The inactive region has the same effective Young's modulus and Poisson's ratio as the rest of the electrode. Fig. 8(b) shows the electrode level stressΣ_{xx} at the end of discharge. We find that the stress inside the elliptic inactive region is uniform, which is consistent with Eshelby's elastic inclusion analysis [34], though here the eigenstrain is caused by an electrochemical process. Note that there is no external load in the x direction. The inactive region itself has caused a large tensile stress with a magnitude of 4 MPa outside the inactive region, especially concentrated around the left and right vertexes of the ellipse where the curvature is high. The generation of this stress can be understood in the following. During discharge, the material surrounding the inactive region expands, while the inactive region does not. Thus the surrounding
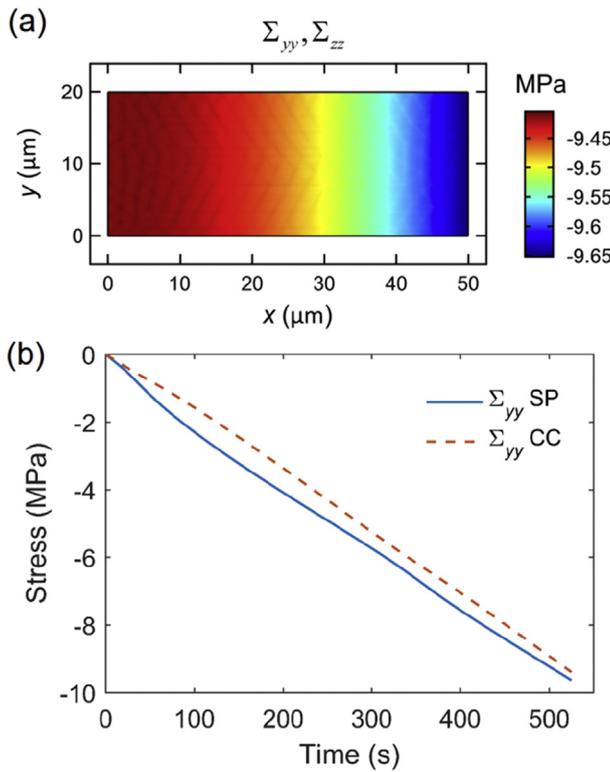
Fig. 6. (a) Distribution of electrode level stress at the end of discharge. (b) Temporal profiles of electrode level stress at positions next to the separator (SP) and next to the current collector (CC).

Fig. 7. Simulated results for the case of $r_p = 1$ μm. (a) Distribution of lithium concentration inside all particles at 200 s; (b) Radial stress distribution in particles at 200 s; (c) Temporal profiles of the electrode level stress next to the separator (SP) and next to the current collector (CC).

material stretches the inactive region, generating stress both inside the inactive region and its vicinity. The generated large tensile stress can lead to cracks in-between particles or loss of electrical connectivity of particles to the network that further extends the inactive region.

To highlight the significance of the electrode level stress, we constructed a representative element composed of active particles and binder, as shown in Fig. 8(c). In the finite element simulation we took Young's modulus of 0.35 GPa and Possion's ratio of 0.34 [8] for the binder that bridges the particles. The volume fraction of binder is 0.1 while the volume fraction of active material is 0.42. With an electrode level stress of 1 MPa applied on the top, the generated local stress in the binder is over 8 MPa, or more than eight times of the electrode level stress. Thus, the electrode level stress of 4 MPa in Fig. 8(b) can result in a local stress more than 32 MPa. Note that tensile strength of polyvinylidene fluoride (PVDF) binder with carbon additives wetted by electrolyte is only 16 MPa [8]. Thus, the level of tensile stress in Fig. 8(b) can easily cause breakage of binder, resulting in further growth of an inactive region or fracture in-between particles. Based on the stress distribution in Fig. 8(b), the favorable growth direction is along the major axis of the elliptical inactive region. This simulation reveals an important mechanism that an electrochemically inactive region can lead to large stress and how an inactive region may grow in an electrode. The finding suggests a strategy to reduce degradation by improving the homogeneity of the electrode.

4. Conclusions

Coupled electrochemical and mechanical modeling can provide important insights on degradation in lithium-ion batteries. Previous efforts have been focused mostly on isolated particles. In this work a multi-scale model is developed to integrate electrochemistry and mechanics at both the particle level and the electrode level with consideration of particle interaction. At the particle level, solid diffusion is modeled using a generalized electrochemical potential, which captures the effects of phase transformation and mechanical stress. The stress in a particle is a superposition of the stress from lithium concentration gradient inside the particle and
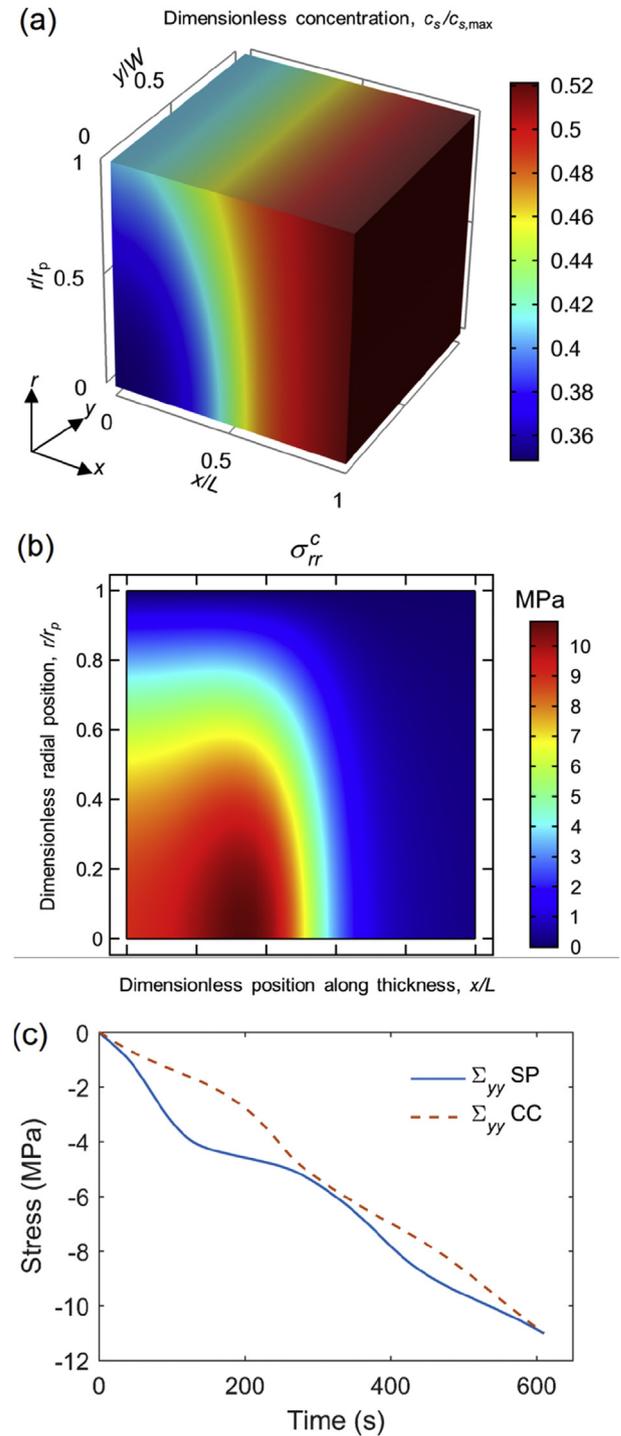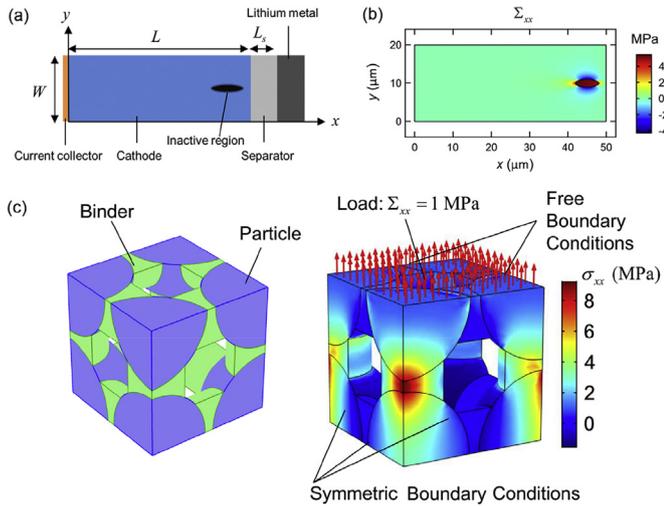
Fig. 8. (a) Schematic of the electrode with an inactive region. (b) Distribution of Σ_{xx} at the end of discharge. (c) Local stress in a representative element.

the stress from particle interaction. Simulation results show that the concentration jump associated with phase transformation can lead to large stress inside particles. Our model highlights that mechanical stress affects both diffusion in the solid and the electrochemical reaction rate between the solid and the electrolyte.

At the continuum electrode level, the effect of mechanical stress on the intercalation current between the solid and the electrolyte is captured by a stress-dependent over-potential. The particle level stress is affected by the electrode level stress. The electrode level stress is calculated on the continuum with effective mechanical properties and the eigenstrains of the RVE. Conceptually, the electrode level stress at a spatial point in the electrode can be viewed as the mechanical loading on an RVE at that point. A relation between the electrode level stress and the particle interaction stress has been developed. While the electrode level stress appears small in comparison to the particle level stress, this electrode level stress can cause severe failure between particles by such as inter-particle fracture since the bonding between particles is much weaker than the cohesion of atoms inside particles.

An important finding we have obtained with this model is a new degradation mechanism, where small electrochemically inactive regions can potentially cause major degradation. We find that the tensile stress generated in the vicinity of an inactive region is large enough to easily break the binder between particles, resulting in fracture or growth of the inactive region. The result points to an approach to reduce degradation by improving the homogeneity of the electrode.

Lithium-ion battery is inherently a multi-scale system. The essence in handling the multi-scale problem lies in the appropriate separation and coupling of different scales. Traditionally, the pseudo-2D electrochemical model separates the electrode level and particle level, and couples the two scales through the charge transfer kinetics at the particle surface. This work has developed a framework to couple the electrochemistry and mechanics at multiple scales simultaneously. Notably, we have introduced a RVE scale between the particle level and the electrode level, enabling the mechanical separation and coupling of the two levels.

Acknowledgement

List of symbols

a_s	Active surface area per unit electrode volume, m^{-1}
c_e	Lithium ion concentration in electrolyte, $mol\ m^{-3}$
c_{e0}	Initial lithium ion concentration in electrolyte, $mol\ m^{-3}$
c_s	Lithium concentration in solid, $mol\ m^{-3}$
c_{s0}	Initial lithium concentration in solid, $mol\ m^{-3}$
$c_{s,max}$	Maximum lithium concentration in solid, $mol\ m^{-3}$
$c_{s,surf}$	Lithium concentration at particle surface, $mol\ m^{-3}$
$\tilde{c}$	Change of lithium concentration from the initial state in solid, $mol\ m^{-3}$
D_e^{eff}	Effective diffusivity of lithium ion in electrolyte phase, $m^2\ s^{-1}$
D_{e0}	Diffusivity of lithium ion in bulk electrolyte, $m^2\ s^{-1}$
D_0	Diffusivity of lithium ion in solid, $m^2\ s^{-1}$
E	Effective Young's modulus of the electrode, GPa
E_p	Young's modulus of the solid particle, GPa
E_{ref}	Open circuit potential, V
$f_\pm$	Electrolyte activity coefficient
F	Faraday's constant, 96485 C mol^{-1}
i	Reaction current density at the surface of the particle, A m^{-2}
i_{app}	Applied current density on the electrode, A m^{-2}
i_0	Exchange current density at the surface of the particle, A m^{-2}
J	Lithium flux in the solid particle, $mol\ m^{-2}\ s^{-1}$
k	Reaction rate constant, $m^{2.5}\ mol^{-0.5}\ s^{-1}$
K	Thermodynamic factor, V
L	Cathode thickness, μm
L_s	Separator thickness, μm
M	Mobility of lithium ion in solid, $m^2\ mol\ J^{-1}$
r	Radial coordinate, μm
r_p	Particle radius, μm
R	Ideal gas constant, 8.314 J $mol^{-1}\ K^{-1}$
t	Time, s
t_+	Lithium ion transference number
T	Temperature, K
u	Radial displacement, μm
W	Side length of the calculated cathode region, μm
x_{Li}	Mole fraction of lithium in the active particle
α	Anodic charge transfer coefficient
$\varepsilon_{rr}, \varepsilon_{\theta\theta}$	Radial and tangential strain in the particle
ε_e	Cathode porosity
$\varepsilon_{e,sep}$	Separator porosity
ε_s	Volume fraction of active material
η	Over-potential, mV
κ_{e0}	Bulk electrolyte conductivity, S m^{-1}
κ_e^{eff}	Effective electrolyte phase conductivity, S m^{-1}
μ	Chemical potential of lithium in solid particle, J mol^{-1}
μ_c	Chemical potential of lithium in solid particle without stress, J mol^{-1}
μ^θ	Chemical potential of lithium in the reference electrode, J mol^{-1}
ν_p	Poisson's ratio of the solid particle
σ_h	Hydrostatic stress, MPa
$\sigma_{rr}, \sigma_{\theta\theta}$	Radial and tangential stress in the particle, MPa
σ_{ij}^c	Stress in the particle induced by lithium concentration gradient, MPa
σ_{ij}^i	Stress in the particle induced by particle interaction, MPa
σ_s^{eff}	Effective solid phase conductivity, S m^{-1}
σ_{s0}	Solid electronic conductivity, S m^{-1}
Σ_{ij}	Electrode level stress, MPa
Φ_e	Electrolyte potential, V
Φ_s	Solid potential, V

Ω Lithium ion partial molar volume, m^3 mol^{-1}

References

[1] J. Vetter, P. Novak, M.R. Wagner, C. Veit, K.C. Moller, J.O. Besenhard, M. Winter, M. Wohlfahrt-Mehrens, C. Vogler, A. Hammouche, J. Power Sources 147 (2005) 269–281.
[2] K. Takahashi, V. Srinivasan, J. Electrochem. Soc. 162 (2015) A635–A645.
[3] J. Christensen, J. Newman, J. Electrochem. Soc. 153 (2006) A1019–A1030.
[4] J. Christensen, J. Newman, J. Solid State Electrochem. 10 (2006) 293–319.
[5] X. Zhang, W. Shyy, A. Marie Sastry, J. Electrochem. Soc. 154 (2007) A910–A916.
[6] I. Laresgoiti, S. Kabitz, M. Ecker, D.U. Sauer, J. Power Sources 300 (2015) 112–122.
[7] R.T. Purkayastha, R.M. McMeeking, Comput. Mech. 50 (2012) 209–227.
[8] K. Takahashi, K. Higa, S. Mair, M. Chintapalli, N. Balsara, V. Srinivasan, J. Electrochem. Soc. 163 (2016) A385–A395.
[9] B. Wu, W. Lu, J. Electrochem. Soc. 163 (2016) A3131–A3139.
[10] J. Park, W. Lu, A.M. Sastry, J. Electrochem. Soc. 158 (2011) A201–A206.
[11] Y. Dai, L. Cai, R.E. White, J. Power Sources 247 (2014) 365–376.
[12] S. Renganathan, G. Sikha, S. Santhanagopalan, R.E. White, J. Electrochem. Soc. 157 (2010) A155–A163.
[13] B. Rieger, S.V. Erhard, K. Rumpf, A. Jossen, J. Electrochem. Soc. 163 (2016) A1566–A1575.
[14] M. Doyle, T.F. Fuller, J. Newman, J. Electrochem. Soc. 140 (1993) 1526–1533.
[15] B. Lu, Y.C. Song, J.Q. Zhang, J. Power Sources 320 (2016) 104–110.
[16] P.K. Leung, C. Moreno, I. Masters, S. Hazra, B. Conde, M.R. Mohamed, R.J. Dashwood, R. Bhagat, J. Power Sources 271 (2014) 82–86.
[17] M. Pharr, Y.S. Choi, D. Lee, K.H. Oh, J.J. Vlassak, J. Power Sources 304 (2016) 164–169.
[18] A.H. Wiedemann, G.M. Goldin, S.A. Barnett, H.Y. Zhu, R.J. Kee, Electrochim. Acta 88 (2013) 580–588.
[19] D.W. Chung, P.R. Shearing, N.P. Brandon, S.J. Harris, R.E. Garcia, J. Electrochem. Soc. 161 (2014) A422–A430.
[20] H. Mendoza, S.A. Roberts, V.E. Brunini, A.M. Grillet, Electrochim. Acta 190 (2016) 1–15.
[21] S.A. Roberts, V.E. Brunini, K.N. Long, A.M. Grillet, J. Electrochem. Soc. 161 (2014) F3052–F3059.
[22] J.D. Eshelby, North-Holland, Amsterdam, in: I.N. Sneddon, R. Hill (Eds.), Progress in Solid Mechanics, 1961, pp. 89–140.
[23] T. Mura, Micromechanics of Defects in Solids, Kluwer Academic Publishers, 1991.
[24] E. Bohn, T. Eckl, M. Kamlah, R. McMeeking, J. Electrochem. Soc. 160 (2013) A1638–A1652.
[25] S. Ghabezloo, Constr. Build. Mater. 24 (2010) 1796–1798.
[26] S. Ghabezloo, in: Poromechanics V: Proceedings of the Fifth Biot Conference on Poromechanics, (2013), pp. 1857–1866.
[27] S. Ghabezloo, J. Sulem, J. Saint-Marc, Cem. Concr. Res. 39 (2009) 54–64.
[28] R. Hill, J. Mech. Phys. Solids 13 (1965) 213–222.
[29] Y. Benveniste, Mech. Mater. 6 (1987) 147–157.
[30] T. Mori, K. Tanaka, Acta Metall. 21 (1973) 571–574.
[31] A.P. Roberts, E.J. Garboczi, J. Am. Ceram. Soc. 83 (2000) 3041–3048.
[32] Z. Hashin, S. Shtrikman, J. Mech. Phys. Solids 11 (1963) 127–140.
[33] T. Hutzenlaub, S. Thiele, N. Paust, R. Spotnitz, R. Zengerle, C. Wachshofer, Electrochimica Acta 115 (2014) 131–139.
[34] J.D. Eshelby, Proc. R. Soc. Lond. Ser. A 241 (1957) 376–396.